

Searching for exotic Higgs bosons from top quark decays at the HL-LHC

Gautam Bhattacharyya,^{a,b)} Indrani Chakraborty,^{d)} Dilip Kumar Ghosh,^{e)} Tapoja Jha,^{e)} Gourab Saha^{a,b,c)}

^{a)} *Saha Institute of Nuclear Physics, 1/AF Bidhan Nagar, Kolkata 700064, India*

^{b)} *Homi Bhabha National Institute, Training School Complex, Anushaktinagar, Mumbai 400094, India*

^{c)} *Universite' de Strasbourg, CNRS, IPHC UMR 7178, Strasbourg, France*

^{d)} *Department of Physics and Material Science and Engineering, Jaypee Institute of Information Technology, A-10, Sector-62, Noida 201307, Uttar Pradesh, India*

^{e)} *School of Physical Sciences, Indian Association for the Cultivation of Science, 2A & 2B, Raja S.C. Mullick Road, Kolkata 700032, India*

E-mail: gautam.bhattacharyya@saha.ac.in, indrani300888@gmail.com,
tpdkg@iacs.res.in, tapoja.phy@gmail.com, gourab.saha@iphc.cnrs.fr

ABSTRACT: Exotic spin-0 states with unusual couplings with the gauge and matter fields of the Standard Model are worth exploring at the CERN LHC. Though our approach is largely model independent, we take inspiration from flavor models based on some discrete symmetries which predict a set of a scalar and a pseudoscalar having purely off-diagonal Yukawa interactions with quarks and leptons. In a previous paper, some of us explored how to decipher such exotic scalar and pseudoscalar states whose off-diagonal Yukawa couplings involve light quarks. In this work we follow a complementary path and focus on the Yukawa couplings that necessarily involve a top quark. If one such spin-0 state is lighter than the top quark, then the rare decay of the latter, on account of the high yield of the $t\bar{t}$ events, could provide a potential hunting ground of those exotic states particularly during the high luminosity phase of the LHC run. We carry out an exhaustive collider analysis of some promising signatures of those exotic states using sophisticated Machine Learning techniques and obtain considerable signal significance.

Contents

I	Introduction	1
II	Selection of signal benchmark points	3
III	Collider Analysis	5
III.1	Monte Carlo simulation of signal and background processes	5
III.2	Pre-selection criteria	6
III.3	Multivariate Analysis	10
III.4	Results	14
IV	Summary and outlook	14

I Introduction

Nonobservation of any new particle so far at the CERN LHC, beyond those which constitute the Standard Model (SM), fuels speculation that our search strategies could be biased towards assuming standard conventional interactions for the nonstandard states. In a previous study [1], some of us explored how to decipher at the LHC the possible existence of light exotic neutral spin-0 states having unconventional gauge and Yukawa interactions. More specifically, we assumed that a relatively light pseudoscalar (χ) and a scalar (H) exist with the following nonstandard properties:

- There are no HVV -type couplings, where $V \equiv W^\pm, Z$. The $H\chi Z$ coupling takes the simple form ($q_\mu \equiv$ momentum transfer, $\theta_W \equiv$ weak angle):

$$H\chi Z : \left(\frac{-ie}{2 \sin \theta_W \cos \theta_W} \right) q_\mu . \quad (\text{I.1})$$

- $H(\chi)$ has *only* flavor off-diagonal Yukawa couplings, with the Yukawa Lagrangian given by

$$Y_{ff'} \bar{f} (i\gamma^5) f' H(\chi) + \text{h.c.} . \quad (\text{I.2})$$

where, $f, f' \equiv e\mu, \mu\tau, e\tau, uc, tc, ut, ds, db, sb$.

Although our approach would be sufficiently model independent, as also mentioned in [1], χ and H with the above properties do emerge as byproducts in a wide class of flavor models which contain three Higgs doublets, e.g. those relying on flavor groups S_3 [2–6] or $\Delta(27)$ [7]. Since there is no HVV coupling and the Yukawa couplings of H and χ remain purely off-diagonal, the LEP2 limit [8] does not apply on the mass of H or χ . Both H and χ can be taken to be light. The parent flavor models from which the above couplings descend generally contain three Higgs doublets, i.e. they contain an additional set of neutral and charged nonstandard scalars than offered by a two Higgs doublet

model. H and χ happen to be the lighter of the two sets of nonstandard CP-even and CP-odd scalars. Although their innate flavor symmetries do not permit VVH coupling, the $ZZ\chi$, $W^\pm H^\mp \chi$ and $W^\pm H^\mp H$ couplings do exist. It is known in a two Higgs doublet context, as demonstrated e.g. in [9], that if the mass splittings between the nonstandard charged and neutral scalar states are within 100 GeV range, the constraint from the electroweak oblique parameters can be comfortably satisfied, provided the absolute masses of those states weigh within a few hundred GeV. It may be noted that a charged Higgs weighing as low as a few hundred GeV is compatible with the LHC data for low $\tan\beta$ with appropriate nonstandard Yukawa couplings. In the context of models with three Higgs doublets, the second set of charged and neutral scalars may be kept a bit heavier (e.g. \sim TeV) and as degenerate as possible to be consistent with electroweak precision constraints [10]. It is also worth noting that the two sets of charged Higgs in a three Higgs doublet scenario may conspire to partially cancel each other's contribution to $b \rightarrow s\gamma$. As a result, a relatively light charged Higgs weighing a few hundred GeV can be accommodated within the radiative B decay constraints [11].

The strategies for uncovering these exotic states were chalked out in Ref. [1] when the relevant off-diagonal Yukawa couplings of χ and H involved only the light quarks. It should be noted that such couplings trigger tree level meson mixing. To avoid stringent constraints from $K^0-\bar{K}^0$ mixing, the χds and $H ds$ couplings were set to zero. An approximate phenomenological relationship between the ratio of χuc and $H uc$ couplings, as proportional to the χ and H masses, was taken to remain consistent with the constraints from $D^0-\bar{D}^0$ mixing. On the leptonic side, the couplings involving the electrons were set to negligible values to avoid constraints from $e^+e^- \rightarrow \mu^+\mu^-(\tau^+\tau^-)$, $\mu-e$ conversion and $\mu \rightarrow e\gamma$ processes. The only relevant leptonic Yukawa interactions involved were $\chi\mu\tau$ and $H\mu\tau$. It was assumed that χ weighs a few tens of a GeV and H is at least 100 GeV heavier than that. The collider study involved production of H dominantly from the parton level uc fusion in pp collision, followed by splitting of H into χ and Z . Eventually, on-shell decays $\chi \rightarrow \mu\tau$ and $Z \rightarrow \ell^+\ell^-$ constituted the final states in Ref. [1]¹.

In the present paper, we perform a complementary study by focusing on the Yukawa couplings involving the top quark, the relevant couplings being Φtj , where $\Phi \equiv H, \chi$ and $j \equiv u, c$. We assume any other quark Yukawa couplings to be extremely small, or vanishing, for the following reasons. Let us recall that the assumption of order 100 GeV neutral scalars with off-diagonal Yukawa couplings calls for special scrutiny from the perspective of constraints on flavor physics, in particular from meson – anti-meson mixing as well as from meson decays, as mentioned also in Ref. [1]. To be specific, setting Φuc couplings below 10^{-4} is enough to keep the contribution to $D^0-\bar{D}^0$ mixing within its saturation limit. If Φtc and Φtu couplings are simultaneously present then they would contribute to $D^0-\bar{D}^0$ mixing at one loop level, but it is safe to assume that their products be less than $\sim 10^{-6}$. Similarly, Φbs couplings of size less than approximately 0.005 would be enough to keep the tree level contribution to $B_s-\bar{B}_s$ mixing within acceptable limit. As regards the leptonic Yukawa couplings, we keep only $\Phi\mu\tau$ as nonvanishing to avoid stringent constraints on couplings involving electrons as stated in Ref. [1]. The numerical hierarchy of all these couplings is in line with the original motivation of reproducing the quark masses and mixing, although actual numbers may vary depending on the specific flavor models and the additional flavon vevs. The spirit of the collider analysis undertaken in the present paper is to take a simplified scenario with a few benchmark points by keeping only those off-diagonal Yukawa couplings as sizable that involve the top quark. A noteworthy point is that S_3 -symmetric flavor models require one of the flavors participating in Yukawa interactions to be necessarily from the third generation, though the off-diagonal Yukawa couplings involving the top quark are unrelated to those involving the bottom quark [2, 3]. With the above in mind, the large production rate of the $t\bar{t}$ pair expected at the high

¹For lepton flavor violating exotic Higgs decays at the LHC/HL-LHC, see also [12, 13]

luminosity run of the LHC (HL-LHC) at 14 TeV gives us motivation to carry out this top-specific exploration.

For simplicity, we assume $m_H > m_t$ and $m_\chi \sim (20 - 100)$ GeV to focus on only one type of exotic state, namely χ , being produced on-shell from top quark decays. Admittedly, our collider analysis is completely blind towards the CP nature of χ . To be specific, we consider one of the pair produced top quarks to decay into W and b , and the other to χ and j , followed by χ decaying to μ and τ . Depending on the hadronic or leptonic decay mode of W^\pm , we focus on two possible signal channels: (a) $1b + 3j + 1\mu + 1\tau_h$ and (b) $1b + 1j + 1\mu + 1\ell$ ($\ell = e, \mu$) + $1\tau_h + \cancel{E}_T$. We consider only the hadronic decay of τ , denoted by τ_h . We use sophisticated Machine Learning techniques for multivariate analysis (MVA) to obtain maximally enhanced signal significance.

The paper is structured as follows. In Section II, we show the Feynman diagrams contributing to our signal events, discuss the constraints on the relevant couplings and mention the benchmark points selected for our studies. Section III contains exhaustive collider analysis of the promising topologies using Machine Learning techniques. We summarize and draw our conclusion in Section IV.

II Selection of signal benchmark points

We probe light exotic spin-0 states coming from flavor violating top quark decays. We rely on the huge production of $t\bar{t}$ events during the HL-LHC run. We assume the CP-even state H to be heavier than the CP-odd state χ and fix m_H to a value larger than m_t , e.g. at 200 GeV. This is to avoid a 2-body decay of t to H and j . But since χ is assumed to be lighter than or equal to 100 GeV, H (and H^+) should not be heavier than few hundred GeV to respect the oblique parameter constraint [14, 15], as stated previously². We have studied the correlation between the oblique parameters [16–18] using the scalar masses in the following ranges : $20 \text{ GeV} \leq m_\chi \leq 100 \text{ GeV}$, $m_H = 200 \text{ GeV}$, $165 \text{ GeV} \leq m_{H^+} \leq 250 \text{ GeV}$. Since the signals only contain the pseudoscalar χ , we have the freedom to adjust m_{H^+} to satisfy the constraints coming from the correlation of the oblique parameters. It could be observed that for $m_\chi = 20 \text{ GeV}$, 60 GeV and 100 GeV, $m_H = 200 \text{ GeV}$ and with proper choice of m_{H^+} within the aforementioned range, the constraints coming from the oblique parameters are comfortably satisfied within 2σ error bar of the experimental limit ($S = 0.05 \pm 0.08$, $T = 0.09 \pm 0.07$, $\rho_{\text{ST}} = 0.92$.) [14, 15]. A point to note is that not only the masses but also the Yukawa couplings of H (as well as of H^+) remain essentially irrelevant for our studies. Our primary focus is on the decay channel $t \rightarrow \chi j$.

Among the different possibilities regarding the signal final states, we analyze only two specific channels involving leptons due to their clean signatures. These are semi-leptonic (SL) and di-leptonic (DL) channels, described below. We focus on one top quark decaying to W boson and b -tagged jets, and the other top quark decaying to χ and a light jet. Subsequently, W can decay to one lepton + \cancel{E}_T or two light jets. To sum up, our final states are

- $b + 3j + \mu + \tau_h$ (SL),
- $b + j + \mu + \tau_h + \ell (= e, \mu) + \cancel{E}_T$ (DL).

The relevant Feynman diagrams are shown in Figure 1.

²Note that the simplified model parameter space we are studying, does not contain any H^\pm , but the inspirational flavor-specific mother models, or for that matter all multi-Higgs models, holistically do. In order to remain conservative, we check consistency with T and S parameters, together with correlations among them, keeping the entire

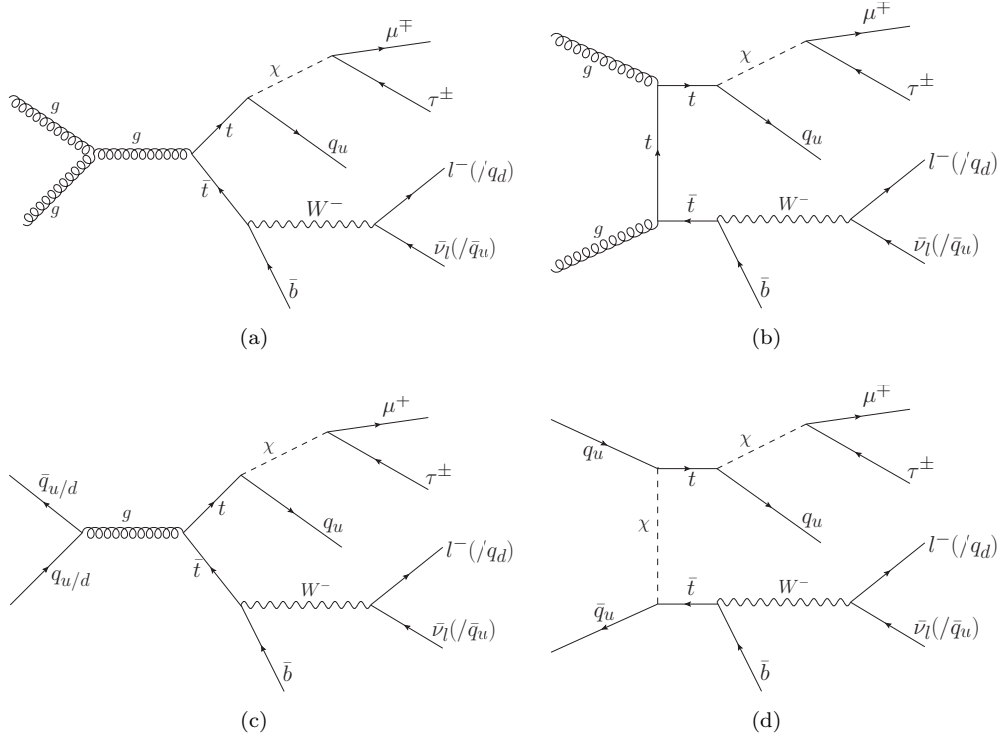


Figure 1: Feynman diagrams of the signal processes in the DL and SL channels. Here, $q_u \equiv u, c$; $q_d \equiv d, s$.

What about the size of the off-diagonal Yukawa couplings of χ ? Is there any guideline from the motivational models? The sizes of the Yukawa couplings of H are related to the entries of the CKM matrix. But the Yukawa couplings of χ are not at all constrained by that as there is no vev in the χ direction. In Ref. [2], the Hct coupling was taken to be approximately 0.8, by assuming that H is heavier than the top quark so that the latter does not have a 2-body decay into H and c . Since the χ is assumed to have a smaller mass than the top quark in our analysis, our benchmark χct coupling has to be significantly smaller. The χtc coupling is varied in the range (0.001 – 0.01). This choice is consistent with the observation that t almost invariably decays to b and W with a branching fraction of 0.998 as per the latest Particle Data Group [19]. If we turn on χtu at the same time, $D^0-\bar{D}^0$ mixing is triggered through one loop box graph forcing the product of χtc and χtu couplings to be at most 10^{-6} . The choices are consistent with the ATLAS and CMS searches for rare top decays [19–24]³. In our scenario, χ decays to μ and τ with almost 100% branching ratio. As a result, though the exact choice of $\chi\mu\tau$ coupling does not matter much, nevertheless we fix it at 0.01. The effective signal cross section can be expressed as: $\sigma_{\text{eff}} = 2 \times \sigma(pp \rightarrow t\bar{t}) \times \text{Br}(t \rightarrow bW) \times \text{Br}(t \rightarrow c\chi) \times \text{Br}(\chi \rightarrow \mu\tau) \times \text{Br}(W \rightarrow \ell\nu/jj)$. The overall factor 2 is a combinatoric factor arising from top (anti-top) decay. We summarize our benchmark values in Table. 1⁴.

scalar multiplets in an extended scenario including the charged Higgs in hindsight, even though the latter does not feature in our specific model independent search domain.

³These searches have set an upper limit on the Branching Ratios (BRs) of rare top decays like $t \rightarrow qh/qg/qZ$, which vary roughly in the range (10^{-2} – 10^{-6}) depending on the final states obtained by extrapolating the 7 TeV LHC data to 14 TeV expectation with 3 ab^{-1} luminosity. In our setup, since we are focusing on the decay channel $t \rightarrow \chi j$ (here j corresponds to light up-type quarks), those search limits are comfortably satisfied by our benchmark coupling range.

⁴It is worth noting that our neutral exotic states (χ and H) cannot be constrained by conventional LHC new

Parameter	Range
m_χ (GeV)	20, 60, 100
$Y_{\mu\tau}^\chi$	0.01
Y_{ct}^χ	0.001 - 0.01

Table 1: Benchmark choices for masses and couplings.

III Collider Analysis

To perform the collider analysis, we first simulate the signal benchmark points (Table 1) and the samples of relevant SM backgrounds (Table 3). After applying a few pre-selection conditions on both signal and background events in order to select coarse signal regions, we proceed to perform MVA techniques. Finally, we estimate the required integrated luminosity to achieve a 5σ discovery and a 2σ exclusion. In the following Subsections, we shall present the details of MVA, which are performed to segregate the signal from corresponding backgrounds for each benchmark point.

III.1 Monte Carlo simulation of signal and background processes

We start our analysis by implementing the Yukawa Lagrangian in **FeynRules** [26] to generate Universal FeynRules Output (UFO). In the next step, the UFO is interfaced with the event generator to simulate the signal. Both the signal and background events are generated using **MadGraph5_aMC@NLO** [27], providing the cross sections at the leading order (LO). It is worth mentioning that in case of signal generation, we have used a factorized approach, and hence ignoring all possible interference effects and irreducible background. The **MadGraph** syntax used for the semi-leptonic and di-leptonic event generation are mentioned in the following:

Semi-leptonic (SL) channel:

```
define p = 21 2 4 1 3 -2 -4 -1 -3 5 -5 # pass to 5 flavors
define j = p
define qu = u u~ c c~
define qd = d d~ s s~ b b~
define ln~ = mu- ta-
define ln = mu+ ta+
generate p p > t t~, (t > qu x, x > ln ln~), (t~ > b~ w-, w- > qu qd)
add process p p > t t~, (t > b w+, w+ > qu qd), (t~ > qu x, x > ln ln~)
output S3_Xmuta_Wjj
```

Di-leptonic (DL) channel:

```
define p = 21 2 4 1 3 -2 -4 -1 -3 5 -5 # pass to 5 flavors
define j = p
define qu = u u~ c c~
define qd = d d~ s s~ b b~
```

scalar search strategies. The primary production mechanism of a neutral scalar at LHC relies on gluon fusion which proceeds through top quark loops. Vector boson fusion and associated productions also leave a sizable contribution to the production. In the absence of a diagonal Yukawa coupling, the gluon fusion mechanism is inoperative. On top of that, the absence of HVV (χVV being absent anyway) switches off the entire conventional mode of production for χ or H search. This is why a standard package like **HiggsTools** [25] is inapplicable for constraining our benchmark points, thus attributing enhanced liberty to the choice of the latter.

```

define ln~ = mu- ta-
define ln = mu+ ta+
define ln1~ = e- mu-
define ln1 = e+ mu+
define vl1 = ve vm
define vl1~ = ve~ vm~
generate p p > t t~, (t > qu x, x > ln ln~), (t~ > b~ w-, w- > ln1~ vl1~)
add process p p > t t~, (t > b w+, w+ > ln1 vl1), (t~ > qu x, x > ln ln~)
output S3_Xmuta_Wlnu

```

For the evaluation of both signal and background cross sections, we employ NN23L01 as the parton distribution function (PDF) [28]. The τ decays are simulated within the TAUOLA package integrated in PYTHIA-8. These parton level events are then passed through PYTHIA-8 [29] for showering and hadronization. To incorporate the detector effects, the resulting events are finally processed through the fast detector simulation package Delphes-3.4.2 [30] using the default CMS card. Within Delphes, we use the anti- k_T jet clustering algorithm [31] using the FastJet package [32]. The respective tagging efficiencies for the b and τ -tagged jets have been parametrically incorporated within the default CMS card.

Among all relevant backgrounds corresponding to two different signal final states SL and DL, the most dominant is the $t\bar{t}$ pair production. This background sample is generated by matching up to two jets. Fully leptonic decays of $t\bar{t}$ pair introduce two leptons in the final state while only one lepton emerges from the semi-leptonic decay of $t\bar{t}$ pair. In addition, associated production of single top with W boson is another significant contributor to the backgrounds. Sizable contributions also arise from $t\bar{t}h$, $t\bar{t}V$, VV , and the QCD-QED $b\bar{b}Z^*/\gamma^* \rightarrow b\bar{b}\tau^+\tau^-$ processes tabulated in Table 3.

III.2 Pre-selection criteria

Relevant acceptance cuts on some of the kinematic variables are required to be applied to identify different particles within the finite size of the detectors. For example, the transverse momentum of each particle (p_T) should be above a particular threshold to maintain optimum identification efficiency. Rejecting the particles with low p_T helps suppress the huge background contributions coming from the QCD processes. Before performing an exhaustive collider analysis, we first apply a set of acceptance cuts (C0) on some of the pertinent kinematic variables as mentioned in Table 2. Although, for signal and for a few background processes (mentioned in Table 3), all these cuts are imposed at the generation level, for some background processes the same cuts are also applied at the analysis level during object selection to keep everything under the same roof. Next, we apply a few more cuts on the lepton and jet multiplicity to achieve the same final state as represented in Figure 1. Below, we describe all the pre-selection cuts (C0 - C5) applied to the signal and background events to select broad signal regions.

C0: The acceptance cuts consist of some basic selection criteria for leptons (e, μ, τ) and jets, imposed on the following set of kinematic variables: (a) transverse momentum p_T , (b) pseudo-rapidity η , and (c) angular separation between i -th and j -th objects $\Delta R_{i,j}$ which is defined in terms of the azimuthal angular separation ($\Delta\phi_{ij}$) and pseudo-rapidity difference ($\Delta\eta_{ij}$) between two objects i and j as $\sqrt{(\Delta\eta_{ij})^2 + (\Delta\phi_{ij})^2}$. The threshold values of these variables are quoted in Table 2.

C1: In both DL and SL channels, χ always decays to $\mu^\pm\tau^\mp$. But W decays leptonically (hadronically) for the DL (SL) channel. We always identify τ through its hadronic decay.

Objects	Selection cuts
e	$p_T > 10 \text{ GeV}, \eta < 2.5$
μ	$p_T > 10 \text{ GeV}, \eta < 2.4, \Delta R_{\mu e} > 0.4$
τ_h	$p_T > 20 \text{ GeV}, \eta < 2.4, \Delta R_{\tau_h, e/\mu} > 0.4$
<i>light jet</i>	$p_T > 20 \text{ GeV}, \eta < 4.7, \Delta R_{\text{light jet}, e/\mu} > 0.4$
<i>b jets</i>	$p_T > 20 \text{ GeV}, \eta < 2.5, \Delta R_{b \text{ jet}, e/\mu} > 0.4$

Table 2: Summary of the acceptance cuts.

Thus for the DL channel, final states each with at least one μ ($e\mu/\mu\mu$) is ensured, whereas for the SL channel, we demand exactly one μ and no e in the final state.

C2: In the final state we require exactly one τ jet, i.e. τ_h , for both the SL and DL channels.

C3: One of the pair produced top quarks in the signal decays to $b(\bar{b})W^-(W^+)$ and the other to χ and a light jet. So, one b tagged jet is required to be present in the final states of both channels. Apart from that, we also apply a cut on the number of light jets. For the DL channel, we demand at least one light jet in the final state, but for the SL analysis, because of the hadronic decay of W , the final state consists of minimum three light jets.

C4: In the DL channel, the signal topology does not allow for a pair of opposite sign same flavor (OSSF) leptons in the final state arising out of the decay of Z -boson. Thus to exclude the Z -peak, we veto the events with a pair of OSSF leptons having an invariant mass $M_{\ell^+\ell^-}$ in the following window: $M_Z - 10 \text{ GeV} < M_{\ell^+\ell^-} < M_Z + 10 \text{ GeV}$.

C5: The next step is to select the leptons and the jets coming from W boson in the DL and SL channels, respectively. As the decay of χ ensures the presence of one μ , the two possible combinations of leptons in the final state are $\mu\mu$ or μe where the second lepton originates from the decay of W in DL channel. While the selection of the μe final state is trivial, it is quite challenging to figure out whether the muon is coming from χ or from W . We first check the distribution of ΔR between τ_h and μ for the μe combination. We observe that in most of the signal events, spatial separation between μ (coming from χ) and τ_h is smaller than that of τ_h and e originating from W . Although this feature is most prominent for the benchmark with the lowest m_χ , it persists for the other two benchmarks as well. For the $\mu\mu$ combination as well the same argument holds. First we choose the μ closer to the τ_h . Then we check if the μ and the τ_h have opposite charges and if it is the case, we consider that μ to be the decay product of χ . Conversely, if they have same charges, we do not reject the event just on that basis. We check if the τ_h and the distant μ have opposite charge. If so, we keep that second μ as the decay product of χ and the first μ as the one coming from W . This algorithm does not guarantee the selection of the perfect combination, still it makes the selection more efficient. To validate this method, the distributions of ΔR between $\mu - \tau_h$ for $\mu\mu$ and μe final states in DL channel are shown in Figure 2. The negligible difference between the distributions prove that this algorithm is exempted from any obvious selection bias. The backgrounds in those plots are: TT +jets, $TT(V)$ +jets and $VV(V)$. The TT +jets contain $t\bar{t} \rightarrow bW$ for SL and DL decay modes; the $T(T)V$ +jets include TV and TTV processes, *e.g.* tW +jets and $t\bar{t}h$; while the $VV(V)$ include the di and tri-boson processes. The μ coming from χ is denoted by μ_χ throughout the rest of the discussion.

For the SL channel, we cannot differentiate whether the jets are coming from t/\bar{t} or from W at first sight. We first compute the invariant mass for each jet pair formed out of all three

Process	cross section (pb)	Yields ($\mathcal{L} = 3 \text{ ab}^{-1}$)	
Signals			
(m_χ, Y_{ct}^χ)	NLO [DL SL]	DL	SL
20, 0.005	0.008 0.026	756	3152.4
20, 0.01	0.033 0.103	2796	11262
60, 0.005	0.012 0.036	2372.4	8696.4
60, 0.01	0.048 0.144	9559.2	34670
100, 0.005	0.007 0.019	1636.8	5733.6
100, 0.01	0.027 0.084	6374	23196.0
SM Backgrounds			
$t\bar{t} \rightarrow 2\ell + jets$	119.34 [NNLO][33]	1057603.13	4314109.11
$t\bar{t} \rightarrow 1\ell + jets$	368.1 [NNLO][33]	7112.07	7334375.95
tW	34.81 [LO]	2463.11	23907.39
$Z \rightarrow \tau^+\tau^- + jets$	803 [NLO]	419.76	20642.35
$t\bar{t}(W \rightarrow \ell\nu) + jets$	0.25 [NLO]	2113.22	8566.4
$t\bar{t}(W \rightarrow qq)$	0.103 (*) [LO]	207.74	2410.91
$t\bar{t}(Z \rightarrow \ell^+\ell^-) + jets$	0.24 [NLO][34]	4228.31	11606.32
$t\bar{t}(Z \rightarrow qq)$	0.206 (*) [NLO][34]	404.22	4729.34
$WZ \rightarrow 3\ell\nu + jets$	2.27 [NLO][35]	2404.83	2688.63
$WZ \rightarrow 2\ell 2q$	4.504 [NLO][35]	1275.99	13659.67
$ZZ \rightarrow 4\ell$	0.187 [NLO][35]	169.42	95.15
$t\bar{t}(h \rightarrow \tau^+\tau^-)$	0.006 (*) [LO]	254.85	661.17
$b\bar{b}\tau^+\tau^-$	0.114 (*) [LO]	36.89	728.65
WWW	0.236 [NLO]	62.0	439.92
WWZ	0.189 [NLO]	47.6	510.03
WZZ	0.064 [NLO]	22.48	159.66
ZZZ	0.016 [NLO]	3.42	18.83
Total background		976565	12692338

Table 3: Event yields at $\mathcal{L} = 3 \text{ ab}^{-1}$ after applying the pre-selection criteria (C0 - C5) for the analyses in both the DL and SL decay channels.

(*): Some selections are applied at the generation (i.e. Madgraph) level. p_T of jets (j) and b quarks (b) $> 20 \text{ GeV}$, p_T of leptons (ℓ) $> 10 \text{ GeV}$, $|\eta|_{j/b} < 5$, $|\eta|_\ell < 2.5$ and $\Delta R_{jj/\ell\ell/j\ell/b\ell} > 0.4$.

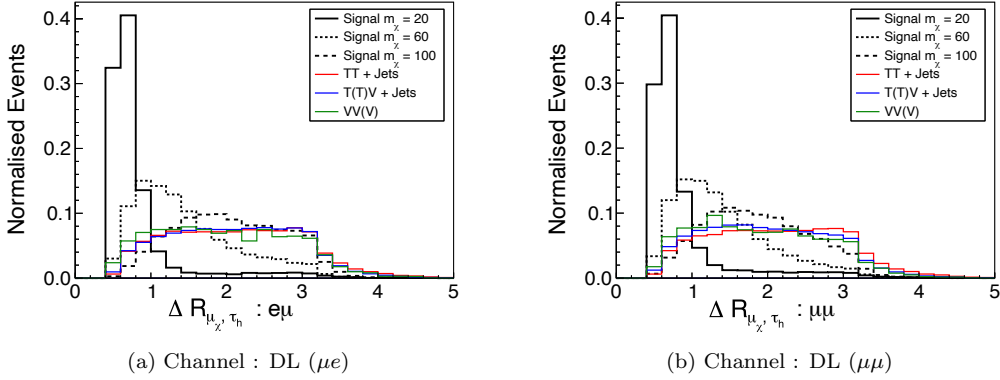


Figure 2: ΔR between μ - τ_h for (a) $e\mu$ (left) and (b) $\mu\mu$ (right) final states of DL channel. Note, $T \equiv t/\bar{t}$, $V \equiv W/Z$.

jets. Then for each event we choose the jet pair having invariant mass closest to M_W (within a 30 GeV window around M_W), and tag the corresponding jet pair as originated from W . From the remaining jets, the leading one is selected as the light jet coming from t/\bar{t} . At the

end, like in the DL channel, we demand that the μ_χ and τ_h must have opposite charges.

After applying the selections mentioned above, we first reconstruct the mass of χ for both channel. For the DL channel, there are two sources of missing transverse energy \cancel{E}_T , i.e. the neutrinos generated in the hadronic decay of τ and those generated from the leptonic decay of W . For SL channel, the single source of \cancel{E}_T is the neutrinos generated from the hadronic decay of τ . Using the collinear approximation [36] for τ decay, we reconstruct the four momentum of τ . The fundamental assumption is that the decay products of τ are boosted in the direction of τ itself since $m_\tau \ll m_\chi$. Thus we take the projection of \cancel{E}_T vector along the direction of τ_h which estimates the p_T of ν_τ . Then we calculate the four momentum of the actual τ by modifying the transverse momentum ($p_T^{\tau_h}$) and energy (E^{τ_h}) of the visible decay product τ_h by the factor $\beta \equiv p_T^{\tau_h} / (p_T^{\tau_h} + p_T^\nu)$. The transverse momentum and energy of the actual τ can be written as :

$$p_T^\tau = \frac{p_T^{\tau_h}}{\beta}, \quad E^\tau = \frac{E^{\tau_h}}{\beta} \quad (\text{III.1})$$

Although this approximation is not expected to yield the most accurate result for the DL channel

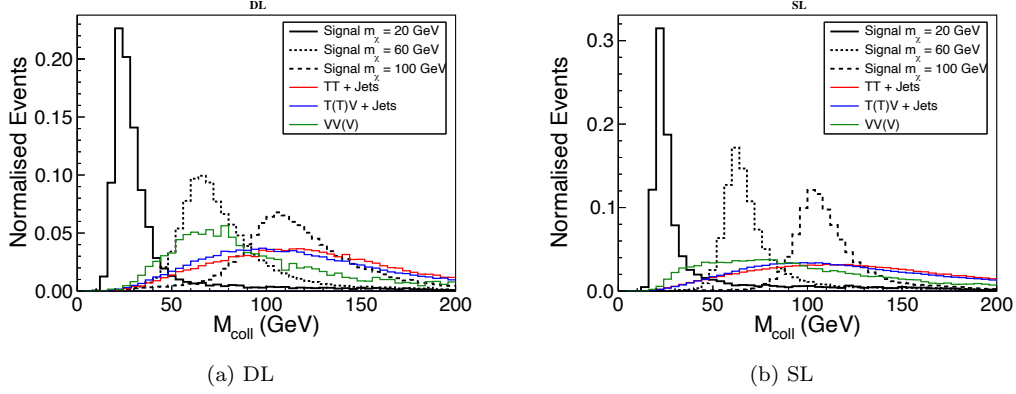


Figure 3: Normalised distributions of collinear mass (M_{coll}) for the (a) DL (left) and (b) SL (right) channels. Note, $T \equiv t/\bar{t}$, $V \equiv W/Z$.

because of two different sources for neutrinos, still we construct the collinear mass M_{coll} of the μ_χ - τ_h system using collinear approximation. In Figure 3, we depict the normalised distributions of M_{coll} for both DL and SL channels. For SL channel, the distributions for different benchmarks peak at $m_\chi = 20, 60$ and 100 GeV, respectively. For the DL channel, the corresponding distributions peak around m_χ , and not exactly at m_χ , for reasons stated above.

A huge number of background events (Table 3) makes it quite challenging to classify the signal events efficiently from the SM backgrounds. Depending on the mass benchmarks, most of the distributions of various kinematic variables show overlapping nature for signals and backgrounds. So, we avoid the traditional cut based method and deploy several MVA techniques to maximize the sensitivity of the analysis. The cross sections of the signals (scaled at next to NNLO+NNLL order by multiplying a k -factor of 1.8 [33]) and the SM background along with their yields after the pre-selection at an integrated luminosity $\mathcal{L} = 3 \text{ ab}^{-1}$ are tabulated in Table 3. Next, we shall briefly describe three different MVA techniques that we employ to maximize the signal significance.

III.3 Multivariate Analysis

Mainly three different MVA techniques, namely, Decorrelated Boosted Decision Tree (BDTD) [37], Extreme Gradient Boost (XGBoost) [38] and Deep Neural Network (DNN) [39] algorithms have been employed to estimate the sensitivity of the signals over the SM backgrounds. For all the three types of MVA techniques, the same set of input variables as mentioned in Table 4 were used. Then we compare the performances of the three methods and use the best one to estimate the signal significance.

Among all the input variables used for training the decision trees or neural network, \cancel{E}_T , p_T of μ_χ and τ_h , $\Delta\phi$ and ΔR between different final state particles, and the scalar sum of transverse momenta of jets (H_T) turn out to be the most important ones⁵. Figure 4 shows the normalised distributions

Variables	Description	DL	SL
$p_T^{\tau_h}, \eta^{\tau_h}$	p_T and η of τ_h	✓	✓
p_T^{bj}, η^{bj}	p_T and η of leading b tagged jet	✓	✓
\cancel{E}_T	Missing transverse energy	✓	✓
p_T^{lj}, η^{lj}	p_T and η of light jet from t/\bar{t}	✓	✓
p_T^{Wj1}, η^{Wj1}	p_T and η of leading jet from W	✗	✓
p_T^{Wj2}, η^{Wj2}	p_T and η of sub leading jet from W	✗	✓
$p_T^{\mu_\chi}, \eta^{\mu_\chi}$	p_T and η of μ coming from χ	✓	✓
$p_T^{W\ell}, \eta^{W\ell}$	p_T of lepton coming from W	✓	✗
$\Delta R_{\mu_\chi, W\ell}$	ΔR between leptons coming from χ and W	✓	✗
$\Delta\phi_{\tau_h, W\ell}$	$\Delta\phi$ between lepton coming from W and τ_h	✓	✗
$\Delta\phi_{bj, W\ell}$	$\Delta\phi$ between lepton coming from W and lead b jet	✓	✗
H_T	Scalar sum p_T of all jets	✓	✓
$\Delta R_{\mu_\chi, \tau_h}$	ΔR between μ and τ_h coming from χ	✓	✓
$m_T^{W\ell, \cancel{E}_T}$	m_T of lepton from W and \cancel{E}_T	✓	✗
$\Delta\phi_{\cancel{E}_T, \mu_\chi}$	$\Delta\phi$ between \cancel{E}_T and the μ from χ	✓	✓
$\Delta\phi_{\cancel{E}_T, W\ell}$	$\Delta\phi$ between \cancel{E}_T and the lepton from W	✓	✗
$\Delta\phi_{\cancel{E}_T, bj}$	$\Delta\phi$ between \cancel{E}_T and leading b jet	✗	✓
$\Delta\phi_{\cancel{E}_T, \tau_h}$	$\Delta\phi$ between \cancel{E}_T and τ_h	✗	✓
$\Delta R_{Wj1, Wj2}$	ΔR between the two jets from W	✗	✓
$m_{\mu, \tau, t\ell j}^{inv}$	Invariant mass of reconstructed τ , μ and light jet from t/\bar{t}	✗	✓
$\sum p_T^{all}$	scalar sum p_T of all the final state particles	✗	✓
$\Delta\phi_{lj, bj}$	$\Delta\phi$ between leading b jet and leading light jet	✓	✓
$\Delta R_{\tau_h, lj}$	ΔR between τ_h and leading light jet	✓	✓
$\sqrt{\hat{s}_{min}}$	Minimum parton level center-of-mass energy	✓	✓
$\cos\theta_{\tau_h, \mu_\chi}^*$	Cosine of the angle between χ and one of its decay products in the rest frame of χ	✓	✓

Table 4: Input variables used(✓) or not(✗) for all of three MVA methods.

of a few important kinematic variables for all three signal mass points and the backgrounds. Figures 4a and 4b show the normalised distributions of ΔR between the τ_h and μ coming from χ for DL and SL channels, respectively. The distributions look similar for both the channels as expected. For $m_\chi = 20$ GeV, the decay products of χ are supposed to be more boosted and hence collimated than the other two benchmark points. That is why the distributions with lower m_χ peak at a lower

⁵Importance of variables is checked by Toolkit for Multivariate Data Analysis (TMVA) variable ranking for BDTD. For DNN and XGBoost, we use permutation method using F-Score [40].

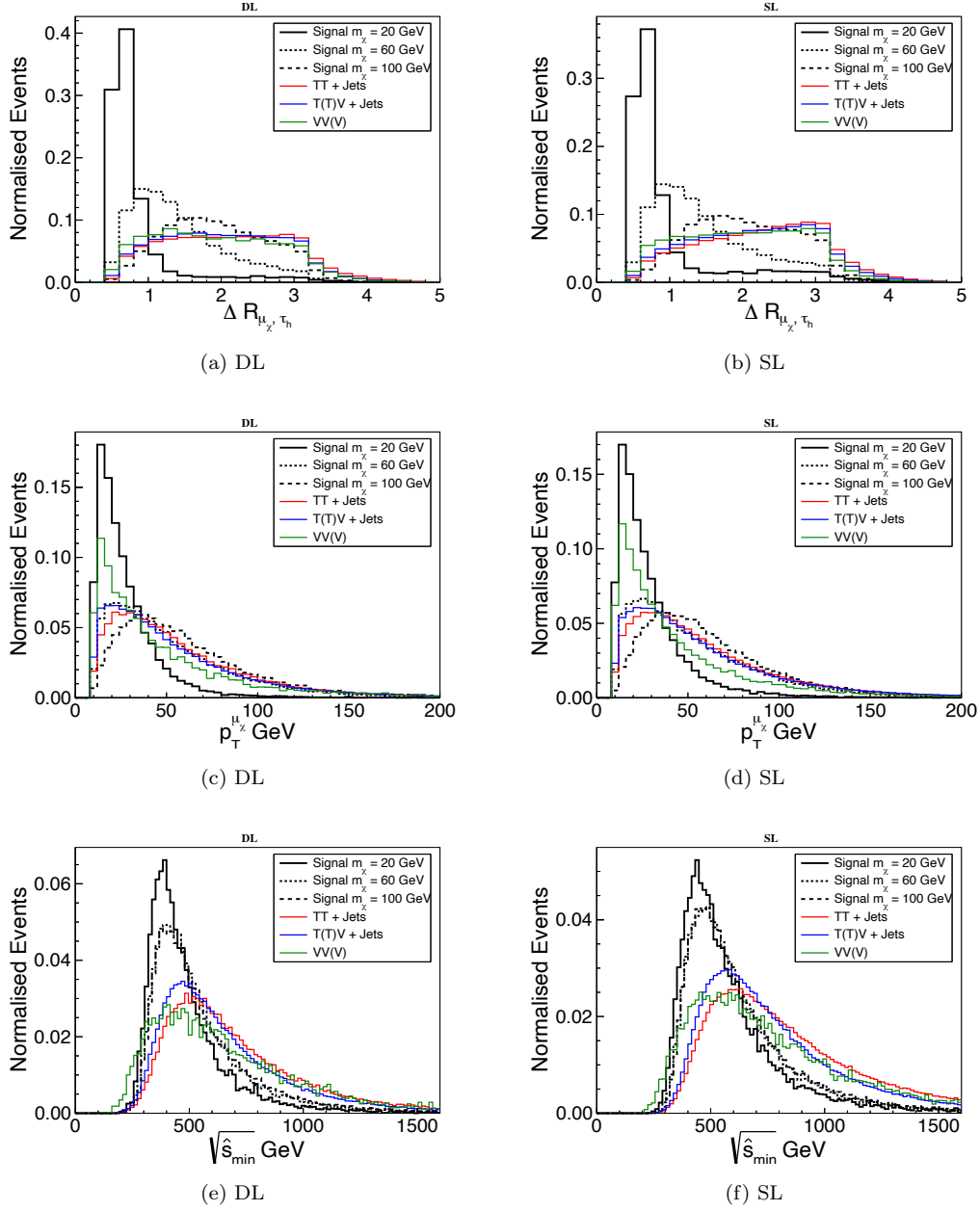


Figure 4: Distributions of some kinematic variables. Column of figures on the left side is for (a) DL channel and (b) SL channel plots are on the right column. The kinematic variables are: (a, b) ΔR between μ_χ and τ_h , (c, d) p_T (in GeV) of μ_χ , and (e, f) $\sqrt{\hat{s}_{min}}$ i.e. minimum parton level center of mass energy for SL and DL channels. Note, $T \equiv t/\bar{t}$, $V \equiv W/Z$.

value of ΔR . Next we present the normalised distributions of another important variable p_T of μ coming from χ for both decay channels in Figure 4c and 4d. The distributions peak towards higher values of p_T for higher values of m_χ as expected. We now mention another important variable: minimum parton level centre-of-mass energy i.e. $\sqrt{\hat{s}_{min}}$ [41] as shown in Figure 4e and 4f. This is a global inclusive variable for determining the mass scale of any new physics in the presence of missing energy in the final states. This variable shows a good discriminating power as well to

identify signals over backgrounds for both the DL and SL channels. In order to minimize any direct dependence on benchmark points, we refrain from utilizing any kinematic variable related to the reconstructed mass of the hypothetical particle that is yet to be seen.

We conduct two-class classification tasks using all three MVA techniques. The "background" class comprises all SM background processes except VVV , while the "signal" class includes signal processes for all considered couplings per mass benchmark. 75% of the total signal and background events are utilized for training. Following this, we evaluate the performances of the respective models using the entire dataset as prior testing on a subset (remaining 25%) results in negligible over-training. Additionally, 20% events from the training set used as a validation set to monitor training performance. As an example, the ratio of the signal (for $m_\chi = 20$ GeV) : background events for SL analysis is around 150000 : 680000 and for DL it is around 125000 : 160000. While combining all the individual background process, we kept a "sample-weight" *i.e.* cross-section/total-events to maintain the ratio of different backgrounds as they should appear in the real data. For signal, we fixed it to 1. At the time of training in *Keras*, we used equal class weights for these signal and background classes on top of using sample-weight, to give equal importance to signal and background classes.

The entire algorithm of BDTD is executed within the TMVA framework [42]. Here, *Adaptive Boost* [43] plays a crucial role for robust and efficient classification. To achieve an optimum performance for each benchmark of both the DL and SL channels, we adjust the parameters of BDTD as described in Table 5. XGBoost is another tree based method like BDTD with some additional

Parameters	Description	Values/Choices		
		$m_\chi = 20$ GeV	$m_\chi = 60$ GeV	$m_\chi = 100$ GeV
n_trees	Number of trees	250	250	250
max_depth	Maximum depth of a Decision Tree	2	2	2
boost	Boosting mechanism for training	AdaBoost	AdaBoost	AdaBoost
n_cuts : SL/DL	Number of iteration to find the best split	50/50	46/31	45/40
min_node_size	Minimum events at each final leaf	2.5%	2.5%	2.5%

Table 5: BDTD parameters used for three different mass benchmark points.

features. Unlike BDTD, it uses *Gradient Boost* for classification. To reduce over-training, some additional parameters are used for pruning a decision tree and regularizing the cost function defined as the difference between the true and predicted output – for details on XGBoost see [38]. Table 6 shows the set of XGBoost parameters used for training the signal and background samples. The third MVA technique that we have employed is Deep Neural Network (DNN). Unlike

Parameters	Description	Values/Choices
booster	Tree based learner	<i>gbtree</i>
n_estimators	Number of decision trees	<i>auto</i>
max_depth	Maximum depth of a Decision Tree	3
η	Learning rate	0.01
λ	Regularization parameter	0.01

Table 6: Details of XGBoost parameters.

decision trees, DNN brings in several hidden layers with multiple nodes. Nonlinear activation functions at the nodes help draw nonlinear boundary on the plane of the DNN variables to separate

signal from background. The complete DNN training has been performed using `keras` module of `tensorflow-2.3.0` [44]. All the parameters used for DNN are in Table 7.

Parameters	Description	Values/Choices
<code>n_hidden layers</code>	Number of hidden layers	5
<code>n_nodes</code>	Number of neurons in hidden layers	512, 256, 128, 54, 8
<code>activation_func</code>	Function to modify outputs of every nodes	<i>LeakyRelu</i>
<code>loss_function</code>	Function to be minimised to get optimum model parameters	<i>binary_crossentropy</i>
<code>optimiser</code>	Perform gradient descent and back propagation	<i>Adam</i> [45]
<code>eta</code>	Learning rate	0.001
<code>batch_len</code>	Number of events in each mini batch	3000
<code>batch_norm</code>	Normalisation of activation output	<i>True</i>
<code>dropout</code>	Fraction of random drop in number of nodes	20%
<code>L2-Regularizer</code>	Regularize loss to prevent overfitting	0.001

Table 7: Details of DNN parameters.

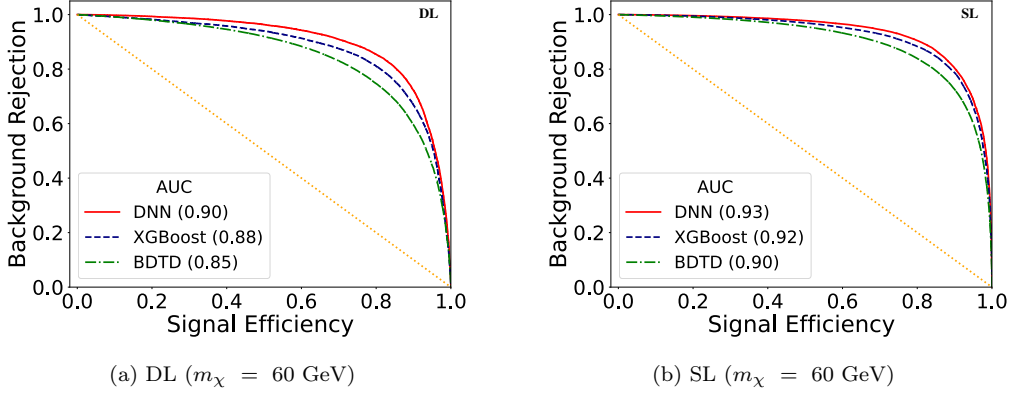


Figure 5: ROCs of three MVA techniques for $m_\chi = 60$ GeV.

All the tree based methods and neural network used in this analysis rely on quite simple architectures. DNN was found to take a bit longer time to finish than the other two methods. Each epoch for DNN was observed to take around 30-45 seconds in a Tesla P100 GPU, while each estimator of XGBoost needed around 10-15 seconds. These three MVA techniques discussed above deliver more or less similar performances. In order to compare their responses, we plot the receiver operating characteristic (ROC) curves for all the three methods and compute the area under the curve (AUC) of each ROC in Figure 5. The degree of performance of the MVA techniques increases with increasing AUC. The comparison shows that the DNN performs somewhat better than BDTD and XGBoost in both the DL and SL channels as reflected in Figure 5 for $m_\chi = 60$ GeV. The other two choices of m_χ exhibit similar behavior. We must admit that no conventional method for hyperparameter tuning has been tried so far for executing these MVA techniques. A proper tuning may change the degree of performances. However, based on the ROC curves obtained here, we shall elaborate the final results only for the DNN technique.

III.4 Results

For evaluation of the signal significance using DNN, we apply suitable cuts on the respective DNN responses that maximize the significance⁶. Then we try to find the required luminosity to achieve a 2σ exclusion and 5σ discovery by scanning over the coupling Y_{ct}^χ . We also estimate the significance after introducing a 5% systematic uncertainty⁷ in total number of background events. The bench-

Classifiers	Signal efficiency (%)				Maximum significance $\mathcal{L} = 3 \text{ ab}^{-1}$
	95	80	65	50	
	Background rejection (%)				
BDTD	49	78	88	93	9.34
XGBoost	59	86	92	95	11.1
DNN	64	89	95	97	14.9

Table 8: A quantitative comparison of the three MVA techniques for the DL channel with $m_\chi = 60 \text{ GeV}$ and $Y_{ct}^\chi = 0.01$.

mark point with $m_\chi = 20 \text{ GeV}$ still shows a good sensitivity after incorporating a 5% systematic uncertainty in the background. The corresponding sensitivity significantly drops for higher m_χ benchmark points – see Figure 6. Lighter the choice of χ the more pronounced is the difference in kinematics of the signal compared to the background – a feature observed for all the three MVA techniques.

Table 8 basically describes the performances of three analysis methods for $m_\chi = 60 \text{ GeV}$ in the DL channel. Here, we just tabulate background rejections for four different signal efficiencies. In addition, the right most column of Table 8 shows the maximum significance at $\mathcal{L} = 3 \text{ ab}^{-1}$.

Now we comment on the search prospects of the three benchmark points at the HL-LHC. In Figure 6, we have drawn 2σ and 5σ contours in the integrated luminosity and Y_{ct}^χ plane with and without considering 5% linear-in-background systematic uncertainty. In Figure 6a and 6b, for $m_\chi = 20 \text{ GeV}$, the 2σ and 5σ contours drawn with 5% systematic uncertainty are shifted towards the higher values of Y_{ct}^χ , thus requiring more luminosity, for the SL channel relative to the DL channel. Benchmarks with $m_\chi = 60 \text{ GeV}$ and $m_\chi = 100 \text{ GeV}$ are accessible to $2\sigma/5\sigma$ significances only with negligible systematic uncertainties. We thus conclude that low m_χ provides promising avenues for exploration both for the DL and SL channels at the HL-LHC. Increasing m_χ lowers the search prospect.

IV Summary and outlook

We have chalked out search strategies for a light exotic pseudoscalar which has only off-diagonal Yukawa interaction with the quarks (tj) and leptons ($\mu\tau$). For this, we have focused on the $t\bar{t}$ production and the subsequent decay channels at the 14 TeV HL-LHC with different luminosities. Large accumulation of $t\bar{t}$ events at the HL-LHC will be a gold mine to study such rare top quark decays. We have adopted a simplified scenario with a minor reference to the big picture based on flavor symmetry models that advocate such nonstandard interaction of the exotic spin-0 states.

⁶For $B \gg S$, the median significance can be simplified as $\mathcal{S} = \frac{S}{\sqrt{B}}$ [46], where S and B are the number of expected signal and background events, respectively. This expression does not take into account systematic uncertainties

⁷In the presence of systematic uncertainty the modified significance is : $\mathcal{S} = \frac{S}{\sqrt{B + (\theta \times B)^2}}$, where θ is the uncertainty (in %) on the number of background events.

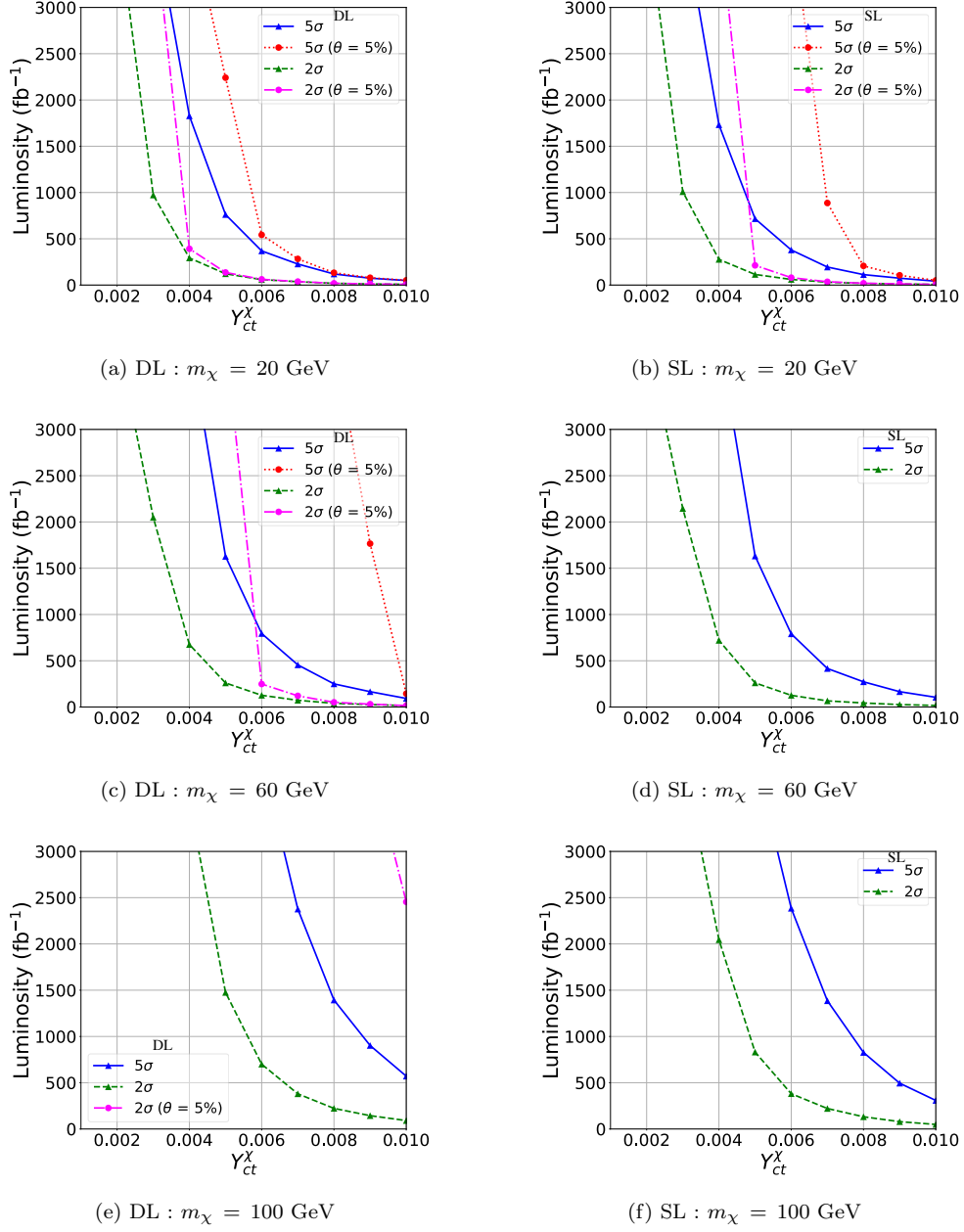


Figure 6: Required integrated luminosity to achieve a 2σ exclusion and 5σ discovery. Figures of the left column correspond to DL channel and figures in the right column correspond to SL channel. Possible systematic uncertainties are expressed through θ .

The present analysis is complementary to a previous study [1] where the off-diagonal couplings of the exotic scalar/pseudoscalar were assumed to involve only lighter quarks. The present analysis focuses on off-diagonal Yukawa couplings involving the top quark. It turns out that uncovering the signal processes from the background is more tricky. We have employed three different Machine Learning techniques to perform multivariate analyses and have found that DNN shows somewhat better performance compared to the other two. No traditional method for hyperparameter tuning has been used.

We admit that our analysis does not take into consideration some technical details, *e.g.* jet faking as τ_h and/or leptons, lepton charge misidentification, photon conversions into lepton pairs, uncertainties on luminosity and trigger efficiencies. Once the real data come, the ATLAS and CMS experimentalists are urged to pursue deeper in this direction.

Acknowledgement

We thank Siddharth Dwivedi, Ipsita Saha and Nivedita Ghosh for useful discussions. IC acknowledges support from DST, India, under grant number IFA18-PH214 (INSPIRE Faculty Award). TJ acknowledges the support from Science and Engineering Research Board (SERB), Government of India under the grant reference no. PDF/2020/001053. We acknowledge support of the computing facilities of Indian Association for the Cultivation of Science and Saha Institute of Nuclear Physics. Finally, we thank the anonymous Referees for their insightful criticisms and suggestions which have led to a substantial improvement of the manuscript.

References

- [1] G. Bhattacharyya, S. Dwivedi, D.K. Ghosh, G. Saha and S. Sarkar, *Searching for exotic Higgs bosons at the LHC*, *Phys. Rev. D* **106** (2022) 055032 [[2202.01068](#)].
- [2] G. Bhattacharyya, P. Leser and H. Pas, *Novel signatures of the Higgs sector from S_3 flavor symmetry*, *Phys. Rev. D* **86** (2012) 036009 [[1206.4202](#)].
- [3] G. Bhattacharyya, P. Leser and H. Pas, *Exotic Higgs boson decay modes as a harbinger of S_3 flavor symmetry*, *Phys. Rev. D* **83** (2011) 011701 [[1006.5597](#)].
- [4] W. Khater, A. Kunčinas, O.M. Ogreid, P. Osland and M.N. Rebelo, *Dark matter in three-Higgs-doublet models with S_3 symmetry*, *JHEP* **01** (2022) 120 [[2108.07026](#)].
- [5] A. Kunčinas, O.M. Ogreid, P. Osland and M.N. Rebelo, *S_3 -inspired three-Higgs-doublet models: A class with a complex vacuum*, *Phys. Rev. D* **101** (2020) 075052 [[2001.01994](#)].
- [6] A. Kunčinas, O.M. Ogreid, P. Osland and M.N. Rebelo, *Dark matter in a CP-violating three-Higgs-doublet model with S_3 symmetry*, *Phys. Rev. D* **106** (2022) 075002 [[2204.05684](#)].
- [7] G. Bhattacharyya, I. de Medeiros Varzielas and P. Leser, *A common origin of fermion mixing and geometrical CP violation, and its test through Higgs physics at the LHC*, *Phys. Rev. Lett.* **109** (2012) 241603 [[1210.0545](#)].
- [8] P. Teixeira-Dias, *Higgs boson searches at LEP*, *J. Phys. Conf. Ser.* **110** (2008) 042030 [[0804.4146](#)].
- [9] G. Bhattacharyya, D. Das, P.B. Pal and M.N. Rebelo, *Scalar sector properties of two-Higgs-doublet models with a global $U(1)$ symmetry*, *JHEP* **10** (2013) 081 [[1308.4297](#)].
- [10] M. Chakraborti, D. Das, M. Levy, S. Mukherjee and I. Saha, *Prospects for light charged scalars in a three-Higgs-doublet model with Z_3 symmetry*, *Phys. Rev. D* **104** (2021) 075033 [[2104.08146](#)].
- [11] R. Boto, J.C. Romão and J.a.P. Silva, *Current bounds on the type-Z Z_3 three-Higgs-doublet model*, *Phys. Rev. D* **104** (2021) 095006 [[2106.11977](#)].
- [12] E. Arganda, X. Marcano, N.I. Mileo, R.A. Morales and A. Szyrkman, *Model-independent search strategy for the lepton-flavor-violating heavy Higgs boson decay to $\tau\mu$ at the LHC*, *Eur. Phys. J. C* **79** (2019) 738 [[1906.08282](#)].
- [13] R.K. Barman, P.S.B. Dev and A. Thapa, *Constraining Lepton Flavor Violating Higgs Couplings at the HL-LHC in the Vector Boson Fusion Channel*, [2210.16287](#).

- [14] C.-T. Lu, L. Wu, Y. Wu and B. Zhu, *Electroweak precision fit and new physics in light of the W boson mass*, *Phys. Rev. D* **106** (2022) 035034 [[2204.03796](#)].
- [15] G. Bélanger, J. Dutta, R.M. Godbole, S. Kraml, M. Mitra, R. Padhan et al., *Revisiting the decoupling limit of the Georgi-Machacek model with a scalar singlet*, [2405.18332](#).
- [16] J.S. Lee and A. Pilaftsis, *Radiative Corrections to Scalar Masses and Mixing in a Scale Invariant Two Higgs Doublet Model*, *Phys. Rev. D* **86** (2012) 035004 [[1201.4891](#)].
- [17] S. Kanemura, Y. Okada, H. Taniguchi and K. Tsumura, *Indirect bounds on heavy scalar masses of the two-Higgs-doublet model in light of recent Higgs boson searches*, *Phys. Lett. B* **704** (2011) 303 [[1108.3297](#)].
- [18] C.-T. Lu, L. Wu, Y. Wu and B. Zhu, *Electroweak precision fit and new physics in light of the w boson mass*, *Phys. Rev. D* **106** (2022) 035034.
- [19] PARTICLE DATA GROUP collaboration, *Review of Particle Physics*, *PTEP* **2022** (2022) 083C01.
- [20] TOP QUARK WORKING GROUP collaboration, *Working Group Report: Top Quark*, in *Community Summer Study 2013: Snowmass on the Mississippi*, 11, 2013 [[1311.2028](#)].
- [21] ATLAS collaboration, *Search for single top-quark production via flavour-changing neutral currents at 8 TeV with the ATLAS detector*, *Eur. Phys. J. C* **76** (2016) 55 [[1509.00294](#)].
- [22] CMS collaboration, *Search for anomalous Wtb couplings and flavour-changing neutral currents in t -channel single top quark production in pp collisions at $\sqrt{s} = 7$ and 8 TeV*, *JHEP* **02** (2017) 028 [[1610.03545](#)].
- [23] ATLAS collaboration, *Search for flavour-changing neutral current top quark decays $t \rightarrow qZ$ in proton-proton collisions at $\sqrt{s} = 13$ TeV with the ATLAS Detector*, .
- [24] CMS collaboration, *Search for associated production of a Z boson with a single top quark and for tZ flavour-changing interactions in pp collisions at $\sqrt{s} = 8$ TeV*, *JHEP* **07** (2017) 003 [[1702.01404](#)].
- [25] H. Bahl, T. Biekötter, S. Heinemeyer, C. Li, S. Paasch, G. Weiglein et al., *HiggsTools: BSM scalar phenomenology with new versions of HiggsBounds and HiggsSignals*, *Comput. Phys. Commun.* **291** (2023) 108803 [[2210.09332](#)].
- [26] A. Alloul, N.D. Christensen, C. Degrande, C. Duhr and B. Fuks, *FeynRules 2.0 - A complete toolbox for tree-level phenomenology*, *Comput. Phys. Commun.* **185** (2014) 2250 [[1310.1921](#)].
- [27] J. Alwall, R. Frederix, S. Frixione, V. Hirschi, F. Maltoni, O. Mattelaer et al., *The automated computation of tree-level and next-to-leading order differential cross sections, and their matching to parton shower simulations*, *JHEP* **07** (2014) 079 [[1405.0301](#)].
- [28] NNPDF collaboration, *Parton distributions for the LHC Run II*, *JHEP* **04** (2015) 040 [[1410.8849](#)].
- [29] T. Sjöstrand, S. Ask, J.R. Christiansen, R. Corke, N. Desai, P. Ilten et al., *An introduction to PYTHIA 8.2*, *Comput. Phys. Commun.* **191** (2015) 159 [[1410.3012](#)].
- [30] DELPHES 3 collaboration, *DELPHES 3, A modular framework for fast simulation of a generic collider experiment*, *JHEP* **02** (2014) 057 [[1307.6346](#)].
- [31] M. Cacciari, G.P. Salam and G. Soyez, *The anti- k_t jet clustering algorithm*, *JHEP* **04** (2008) 063 [[0802.1189](#)].
- [32] M. Cacciari, G.P. Salam and G. Soyez, *FastJet User Manual*, *Eur. Phys. J. C* **72** (2012) 1896 [[1111.6097](#)].
- [33] “Nnlo+nnll top-quark-pair cross sections.”
<https://twiki.cern.ch/twiki/bin/view/LHCPhysics/TtbarNNLO>.
- [34] A. Kardos, Z. Trocsanyi and C. Papadopoulos, *Top quark pair production in association with a Z -boson at NLO accuracy*, *Phys. Rev. D* **85** (2012) 054015 [[1111.0610](#)].

- [35] J.M. Campbell, R.K. Ellis and C. Williams, *Vector boson pair production at the LHC*, *JHEP* **07** (2011) 018 [[1105.0020](#)].
- [36] R. Ellis, I. Hinchliffe, M. Soldate and J. Van Der Bij, *Higgs decay to $\tau^+\tau^-$ a possible signature of intermediate mass higgs bosons at high energy hadron colliders*, *Nuclear Physics B* **297** (1988) 221.
- [37] B.P. Roe, H.-J. Yang, J. Zhu, Y. Liu, I. Stancu and G. McGregor, *Boosted decision trees, an alternative to artificial neural networks*, *Nucl. Instrum. Meth. A* **543** (2005) 577 [[physics/0408124](#)].
- [38] T. Chen and C. Guestrin, *XGBoost: A scalable tree boosting system*, in *Proceedings of the 22nd ACM SIGKDD International Conference on Knowledge Discovery and Data Mining*, KDD '16, (New York, NY, USA), pp. 785–794, ACM, 2016, [DOI](#).
- [39] Y. LeCun, Y. Bengio and G. Hinton, *Deep learning*, *nature* **521** (2015) 436.
- [40] L. Breiman, *Random forests*, *Machine Learning* **45** (2001) 5.
- [41] P. Konar, K. Kong and K.T. Matchev, \sqrt{s}_{min} : A Global inclusive variable for determining the mass scale of new physics in events with missing energy at hadron colliders, *JHEP* **03** (2009) 085 [[0812.1042](#)].
- [42] A. Hocker et al., *TMVA - Toolkit for Multivariate Data Analysis*, [physics/0703039](#).
- [43] Y. Freund and R.E. Schapire, *A decision-theoretic generalization of on-line learning and an application to boosting*, *Journal of Computer and System Sciences* **55** (1997) 119.
- [44] M. Abadi, A. Agarwal, P. Barham, E. Brevdo, Z. Chen, C. Citro et al., *TensorFlow: Large-scale machine learning on heterogeneous systems*, 2015.
- [45] D.P. Kingma and J. Ba, *Adam: A Method for Stochastic Optimization*, 12, 2014 [[1412.6980](#)].
- [46] G. Cowan, K. Cranmer, E. Gross and O. Vitells, *Asymptotic formulae for likelihood-based tests of new physics*, *Eur. Phys. J. C* **71** (2011) 1554 [[1007.1727](#)].